



PtNPs-GNPs-MWCNTs- β -CD nanocomposite modified glassy carbon electrode for sensitive electrochemical detection of folic acid

Meng-Meng Yuan¹ · Jiao Zou¹ · Zhao-Ning Huang¹ · Dong-Ming Peng² · Jin-Gang Yu¹

Received: 19 November 2019 / Revised: 28 January 2020 / Accepted: 3 February 2020 / Published online: 11 March 2020
© Springer-Verlag GmbH Germany, part of Springer Nature 2020

Abstract

A novel electrochemical sensor, platinum nanoparticles/graphene nanoplatelets/multi-walled carbon nanotubes/ β -cyclodextrin composite (PtNPs-GNPs-MWCNTs- β -CD) modified carbon glass electrode (GCE), was fabricated and used for the sensitive detection of folic acid (FA). The PtNPs-GNPs-MWCNTs- β -CD nanocomposite was easily prepared with an ultrasound-assisted assembly method, and it was characterized by scanning electron microscopy (SEM) and transmission electron microscopy (TEM). The electrochemical behavior of FA at PtNPs-GNPs-MWCNTs- β -CD/GCE was investigated in detail. Some key experimental parameters such as pH, amount of PtNPs-GNPs-MWCNTs- β -CD composite, and scan rate were optimized. A good linear relationship ($R^2 = 0.9942$) between peak current of cyclic voltammetry (CV) and FA concentration in the range 0.02–0.50 mmol L⁻¹ was observed at PtNPs-GNPs-MWCNTs- β -CD/GCE. The detection limit was 0.48 μ mol L⁻¹ (signal-to-noise ratio = 3). A recovery of 97.55–102.96% was obtained for the determination of FA in FA pills (containing 0.4 mg FA per pill) at PtNPs-GNPs-MWCNTs- β -CD/GCE, indicating that the modified electrode possessed relatively high sensitivity and stability for the determination of FA in real samples.

Keywords Cyclic voltammetry · Electrochemical detection · Folic acid · PtNPs-GNPs-MWCNTs- β -CD

Introduction

Folic acid (FA), a B vitamin, is water soluble and has a major role in biological functions [1]. Folate deficiency causes megaloblastic anemia and subclinical deficiency, chronic liver disease, biochemical and hematologic lesions, and birth defects [2]. In contrast, high doses of FA during pregnancy are associated with low weight for gestational age at birth [3]. Therefore, the rapid and accurate measurement of FA and the assessment of its folate nutritional status are really

important. Liquid chromatography–ion chromatography (LC-IC) [4], fluorescent probe [5], LC–tandem mass spectrometry (LC-MS/MS) [6], surface plasmon resonance [7], and so on have been developed for the detection or determination of FA. In particular, electrochemical methods have attracted increasing attention due to their advantages such as speed, precision, lower reagent usage, and lower equipment costs compared with certain analytical techniques [8, 9]. For example, cobalt oxide–reduced graphene oxide–cetyltrimethyl ammonium bromide modified carbon paste electrode (Co₃O₄-rGO-CTAB/CPE) was fabricated for sensing FA in real samples by differential pulse voltammetry (DPV) [10]; three-dimensional (3D) rGO/FeNi₃–ionic liquid nanocomposite modified CPE showed excellent electrocatalytic properties towards FA owing to the synergistic effects of the two components [11]; carbon black (CB), GO, copper nanoparticles (CuNPs), and poly(3,4-ethylenedioxythiophene)-poly(styrenesulfonate) (PEDOT:PSS) composite was prepared by ultrasonic agitation and used as electrode modifier for detection of FA by square-wave voltammetry (SWV) [12]; graphene/ZnO nanowire

Meng-Meng Yuan and Jiao Zou contributed equally to this work.

- ✉ Dong-Ming Peng
pdmcsu@126.com
- ✉ Jin-Gang Yu
yujg@csu.edu.cn

¹ College of Chemistry and Chemical Engineering, Central South University, Changsha 410083, Hunan, China

² School of Pharmacy, Hunan University of Chinese Medicine, Changsha 410208, Hunan, China

arrays/graphene foam modified glassy carbon electrode was used for determination of FA in tablets and urine [13]. Thus, the development of fast and facile sensing systems for the measurement of FA in real samples is an ongoing, active area of research [14].

Cyclodextrins (CDs) are a well-known series of cyclic oligosaccharides containing 6–12 D-glucopyranose units [15]. CDs exhibit some special properties such as a hydrophobic cavity of different sizes, natural chirality, and external hydrophilicity. Many organic and inorganic compounds can be embedded into the hydrophobic cavity of CDs [16]. To some extent, the physicochemical properties of the encapsulated materials can be changed a lot [17]. That is to say, functional CD-based molecular recognition can be obtained owing to the possibility of formation of inclusion complexes between inorganic/organic substances and CDs; this has also been beneficial to their wide application in electrochemical recognition [18, 19]. β -CD containing seven glucopyranose units with a cavity size suitable for accommodating aromatic rings and it readily forms an inclusion complex (IC) with FA [20]. β -CD is widely used as a dispersing agent for insoluble chemicals and nanomaterials [21]. In addition, nanocomposites composed of β -CD also exhibited high stability and could be used in highly efficient electrochemical recognition due to the synergistic effects of the nanoparticles and β -CD [22].

Being composed of carbon atoms which form one-dimensional (1D) systems with nanostructures, carbon nanotubes (CNTs) have shown some specific properties such as high thermal stability, excellent conductivity, huge surface area, and relatively high mechanical and chemical capability. CNTs are classified into two types, multi-walled CNTs (MWCNTs) and single-walled CNTs (SWCNTs), according to the number of carbon atom layers [23]. CNT-based sensors were developed and they have many advantages such as high sensitivity and selectivity. Fe_3O_4 /multi-walled carbon nanotubes (Fe_3O_4 /MWCNTs) and Fe_3O_4 /fluorinated MWCNTs (Fe_3O_4 /F-MWCNTs) nanocomposite modified electrodes were used for the sensitive, selective, and simultaneous electrochemical detection of multiple heavy metals in the environment [24]; a nanostructured silver-doped TiO_2 /CNTs hybrid-based sensor was used as a sensitive sensor for electrochemical detection of cetirizine [25]; an MWCNT- SiO_2 @Au core-shell nanocomposite-based sensor was used for ultrasensitive detection of bisphenol A, indicating that MWCNTs could be used as efficient electrode modifiers [26].

Graphene, a sheet-like structure containing one or multiple layers of six-membered carbon rings [27, 28], possesses a two-dimensional (2D) honeycomb lattice structure. Up to now, graphene has become a basic unit of many novel nanocomposites. The carbon atoms on the graphene are sp^2 hybridized, which contributes a lot to its relatively high conductivity [29]. Various graphene oxide (GO) or graphene-based sensors were developed for selective electrocatalytic recognition

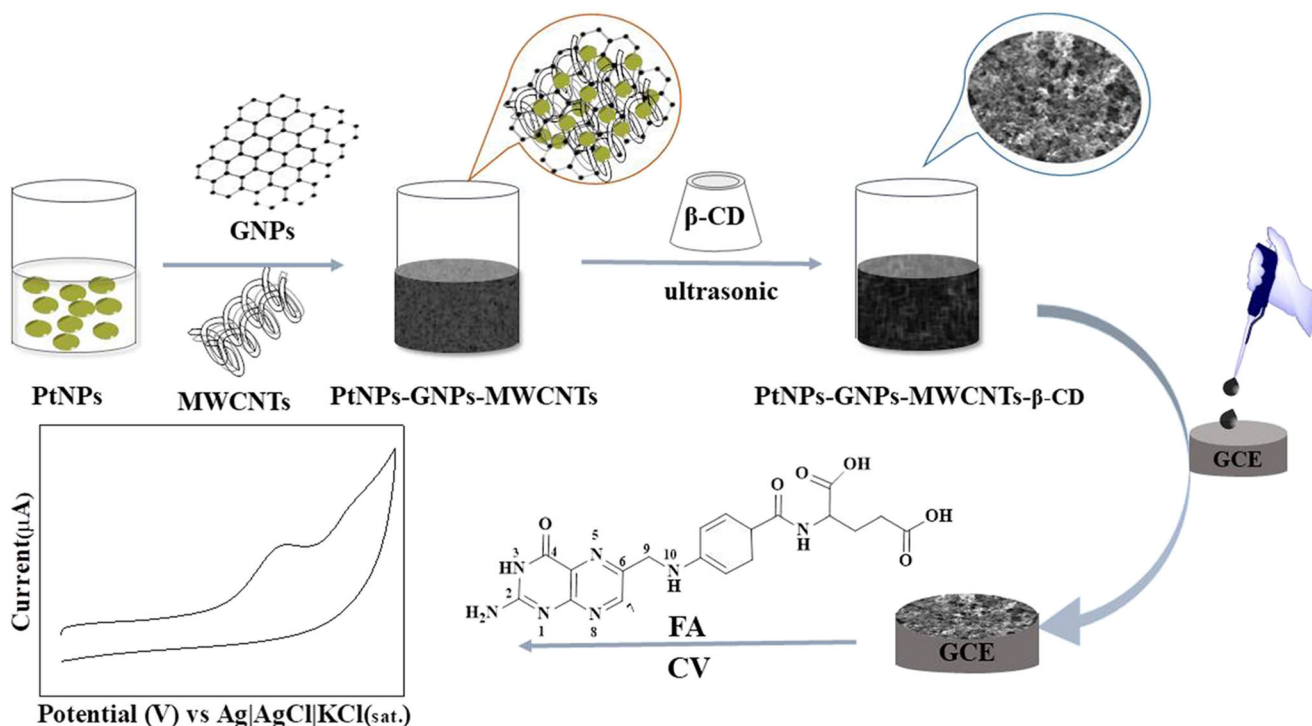
[30–32]. Novel composite materials fabricated by the combination of graphene or GO or graphene nanoplatelets (GNPs) with noble metal nanoparticles (NMNPs) such as gold nanoparticle (AuNPs) [33], platinum nanochains (PNCs) [34], platinum nanoparticles (PtNPs), and so on have been shown to be very effective.

Herein, a PtNPs-GNPs-MWCNTs- β -CD nanocomposite was fabricated through a facile ultrasound-assisted assembly method. The nanocomposite combines the advantages of β -CD, PtNPs, GNPs, and MWCNTs such as good conductivity, large specific surface area, and excellent inclusion properties. The electrocatalytic properties of PtNPs-GNPs-MWCNTs- β -CD nanocomposites modified carbon glass electrode (PtNPs-GNPs-MWCNTs- β -CD/GCE) toward FA was evaluated by cyclic voltammetry (CV) (Scheme 1). The application of PtNPs-GNPs-MWCNTs- β -CD/GCE in detection of FA in real samples was also investigated.

Materials and methods

Materials and apparatus

FA (99 wt%) and β -CD (B.R.) were purchased from Tokyo Chemical Industry Co, Ltd. (Shanghai, China). Chloroplatinic acid hexahydrate ($\text{H}_2\text{PtCl}_6 \cdot 6\text{H}_2\text{O}$, 99.95 wt%), sodium citrate, and glutamate were provided by Aladdin Industrial Co., Ltd. (Shanghai, China). GNPs (99.5 wt%) and MWCNTs (> 95 wt%) were provided by Nanjing Xianfeng Nano Technology Co., Ltd. (Nanjing, China). Potassium ferricyanide ($\text{K}_3[\text{Fe}(\text{CN})_6]$, $\geq 99.5\%$ wt%) was obtained from Tianjin Broadcom Chemical Co., Ltd. (Tianjin, China). Disodium hydrogen phosphate dodecahydrate ($\text{Na}_2\text{HPO}_4 \cdot 12\text{H}_2\text{O}$, $\geq 99.5\%$ wt%), sodium dihydrogen phosphate dihydrate ($\text{NaH}_2\text{PO}_4 \cdot 2\text{H}_2\text{O}$, $\geq 99.5\%$ wt%), phosphoric acid (H_3PO_4 , 98 wt%), sodium hydroxide (NaOH , $\geq 96.0\%$ wt%), sodium chloride (NaCl , $\geq 99.5\%$ wt%), potassium chloride (KCl , $\geq 99.5\%$ wt%), magnesium chloride (MgCl_2 , $\geq 98.0\%$ wt%), zinc nitrate ($\text{Zn}(\text{NO}_3)_2$, $\geq 99.0\%$ wt%) and calcium chloride (CaCl_2 , $\geq 96.0\%$ wt%) were purchased from Sinopharm Chemical Reagent Co., Ltd. (Shanghai, China). Glucose ($\text{C}_6\text{H}_{12}\text{O}_6 \cdot \text{H}_2\text{O}$, A.R.) was purchased from Tianjin Heng Xing Chemical Co., Ltd. (Tianjin, China). Folic acid tablets were obtained from Tianjin Feiying Pharmaceutical Co., Ltd. (Tianjin, China). Alumina polishing powder (Al_2O_3 , 0.05 μm) was purchased from Lab Testing Technology Co., Ltd. (Shanghai, China). All of the solutions were freshly prepared using high-purity water with an electrical resistivity of 18.2 $\text{M}\Omega \text{ cm}$, which was produced by a Millipore Milli-Q water purification system (Millipore Trading Co., Ltd.; Shanghai, China). A thermal heating magnetic mixer (DF-101S; Gongyi Yuhua Instrument Co., Ltd., China), a centrifugal machine (TGL-16GA; Zhengzhou Changcheng Science



Scheme 1 Fabrication of PtNPs-GNPs-MWCNTs- β -CD/GCE and its electrochemical behavior toward FA

Industry & Trade Co., Ltd., China), and an ultrasonic cleaner with an output power of 250 W (SB-100D; 40 kHz; Ningbo Scientz Biotechnology Co., Ltd., China) was used to fabricate PtNPs and the PtNPs-GNPs-MWCNTs- β -CD composite.

Synthesis of PtNPs

PtNPs with average particle sizes of 3.5–5.2 nm were prepared according to the previously reported method [35]. Thus, 100.0 mL of $\text{H}_2\text{PtCl}_6 \cdot 6\text{H}_2\text{O}$ (1.0 mmol L^{-1}) solution was heated to 110°C , and then 10.0 mL of aqueous sodium citrate (38.8 mmol L^{-1}) was added into the reaction. After 30 min, the solution turned black. The solution was stirred for another 10 min and then allowed to cool to room temperature. The mixture was rinsed twice with high-purity water and centrifuged, and the residual solid was dispersed in 25.0 mL of high-purity water to obtain aqueous PtNPs dispersion, which was stored in a refrigerator at 4°C for future use.

Fabrication of PtNPs-GNPs-MWCNTs- β -CD composite modified electrode

A homogeneous dispersion of 4.0 mg of GNPs, 4.0 mg of MWCNTs, and 2.0 mL of PtNPs was prepared by 250-W ultrasound treatment in ultrapure water. After 100 μL of aqueous β -CD (2.0 mg mL^{-1}) solution was added into the reaction, it was sonicated for another 10 min to obtain assembled PtNPs-GNPs-MWCNT- β -CD composite.

Bare GCE was polished with alumina ($0.05 \mu\text{m}$) slurries and then sonicated in water for 3 min. After it was dried in a stream of nitrogen (N_2), PtNPs-GNPs-MWCNTs- β -CD suspension with different volumes was dropped onto the surface of the GCE and allowed to dry to obtain PtNPs-GNPs-MWCNTs- β -CD/GCE.

Electrochemical measurements

Each sample was measured three times consecutively to evaluate the reproducibility of the modified electrodes, and relative standard deviation ($\text{RSD} = \text{standard deviation}/\text{mean} \times 100\%$, $n = 3$) was calculated. Electrochemical experiments were carried out on a CHI660E Electrochemical Workstation (Chenhua Instrument Co., Ltd.; Shanghai, China) with a classical three-electrode system which contained a Pt auxiliary electrode, an $\text{Ag}|\text{AgCl}|\text{KCl}_{(\text{sat.})}$ reference electrode, and a working electrode.

Characterization

The microstructure and morphology of the samples were characterized using a high-resolution transmission electron microscope (HR-TEM, JEM-2100F, JEOL Ltd., Tokyo, Japan), a field emission scanning electron microscope (FE-SEM, TESCAN MIRA3 LMH/LMU, Czech), and an atomic force microscope (AFM, Bruker Dimension Icon, operating in tapping mode, USA). The functional groups of materials were also characterized by Fourier transform infrared spectroscopy

(FT-IR, Perkin Elmer Spectrum 100, USA). Raman spectra were recorded at room temperature with a confocal micro-Raman spectrometer (Horiba LabRAM HR 800, UK).

Results and discussion

Characterization of materials

Morphological analyses

The morphology of PtNPs was investigated by HR-TEM. As shown in Fig. 1, the PtNPs were monodisperse with particle sizes of 3.5–5.2 nm. Furthermore, ordered lattices of PtNPs could also be found. As shown in Fig. 1b, the d spacing of adjacent fringes for PtNPs is 0.227 nm, which corresponds to the (111) crystal plane of face-centered cubic (fcc) Pt phase (Fig. 1b) [36, 37].

The morphology of PtNPs-GNPs-MWCNTs- β -CD was observed by FE-SEM. Figure 2 shows that the PtNPs-GNPs-MWCNTs- β -CD composite possesses a loose, porous, and rough structure due to the ultrasound-assisted assembly of PtNPs, GNPs, MWCNTs, and β -CD. It is proposed that more effective electron transfer between a modified electrode with porous interface and an analyte could be facilitated, thereby greatly improving the electrochemical responses [38].

The surface characteristics of the developed sensor were investigated by using AFM. As shown in Fig. 3a, bare GCE possessed a homogeneous structure and low-roughness features (3.87 nm). Compared to bare GCE, a 100-fold dilution of the PtNPs-GNPs-MWCNTs- β -CD composite modified GCE showed higher surface roughness (7.05 nm) (Fig. 3b), again indicating that the PtNPs-GNPs-MWCNTs- β -CD composite possessed a loose and porous structure. The AFM analyses were consistent with the SEM results.

FT-IR spectroscopy

GNPs, MWCNTs, β -CD, and PtNPs-GNPs-MWCNTs- β -CD were characterized by FT-IR spectroscopy (Fig. 4). GNPs, MWCNTs, and β -CD exhibited characteristic absorption

peaks at ca. 3421 cm^{-1} , which correspond to the stretching vibration of O–H bonds, and ca. 1075 cm^{-1} , which could be attributed to the asymmetric stretching vibration of C–O bonds. In addition, β -CD showed typical absorption peaks at 2910 cm^{-1} , 1395 cm^{-1} , and 1640 cm^{-1} which could be ascribed to the stretching vibration and bending vibration of C–H bonds, and the bending vibration of O–H bonds, respectively. After assembly, the PtNPs-GNPs-MWCNTs- β -CD composite also showed the corresponding absorption peaks as those of GNPs, β -CD, and MWCNTs with slight wavenumber shifts, indicating possible intermolecular interactions among the components [39].

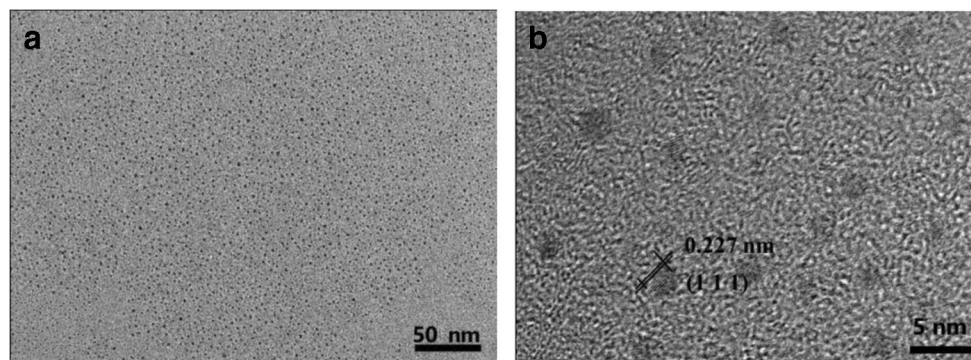
Raman spectroscopy

In order to reveal more structural information about the composite, Raman spectra were recorded. The spectra of GNPs, MWCNTs, and PtNPs-GNPs-MWCNTs- β -CD in Fig. 5 each contain two characteristic peaks: the D band at 1348 cm^{-1} corresponds to the vibrations of carbon atoms with dangling bonds in the graphene edge (or a graphene piece that contains defects), and the G band at 1577 cm^{-1} represents the vibration of sp^2 hybrid carbon atoms in a two-dimensional hexagonal lattice. The intensity ratio of D band and G band (I_D/I_G) is usually used to evaluate the degree of disorders or defects of carbon-based materials [40]. The I_D/I_G values of GNPs and MWCNTs were 0.19 and 1.07, respectively, confirming the fewer defects or disorders in these two kinds of pristine carbon nanomaterials. The I_D/I_G value of PtNPs-GNPs-MWCNTs- β -CD is 0.27, which was between the values of GNPs and MWCNTs, indicating that the obtained PtNPs-GNPs-MWCNTs- β -CD composite possessed an integrated structure of GNPs and MWCNTs. Meanwhile, the other two components, PtNPs and β -CD, which were assembled with GNPs and MWCNTs, had a small effect on the I_D/I_G value [41].

Electrochemical properties of modified electrodes

Figure 6A presents cyclic voltammograms of bare GCE, PtNPs/GCE, GNPs/GCE, MWCNTs/GCE, β -CD/GCE,

Fig. 1 HR-TEM images of PtNPs. **a** Low resolution. **b** High resolution



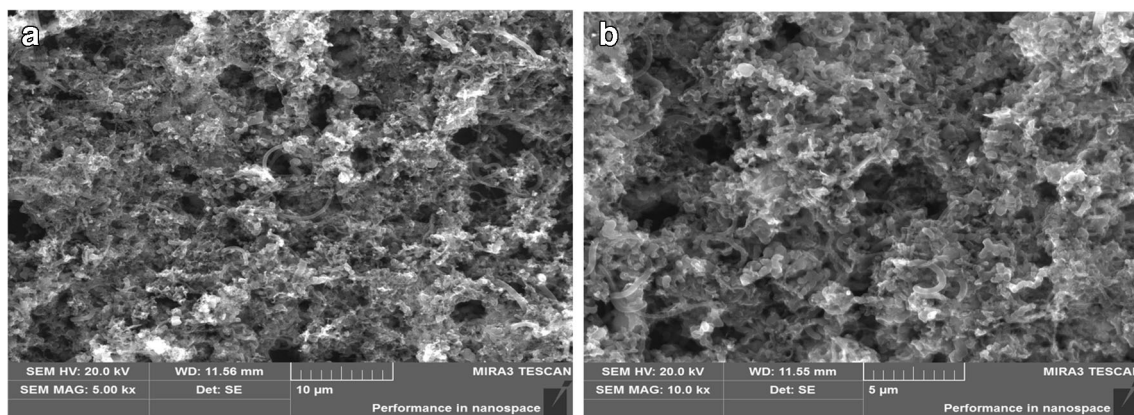


Fig. 2 FE-SEM images of PtNPs-GNPs-MWCNTs- β -CD composite. **a** Low resolution. **b** High resolution

PtNPs-GNPs-MWCNTs/GCE, and PtNPs-GNPs-MWCNTs- β -CD/GCE in $1.0 \text{ mmol L}^{-1} \text{ K}_3\text{Fe}(\text{CN})_6$ in $0.1 \text{ mol L}^{-1} \text{ KCl}$. The peak currents of bare GCE, PtNPs/GCE, GNPs/GCE, MWCNTs/GCE, β -CD/GCE, PtNPs-GNPs-MWCNTs/GCE, and PtNPs-GNPs-MWCNTs- β -CD/GCE gradually increased: 5.59, 7.68, 8.57, 9.37, 10.41, 12.75, and 14.25 μA , respectively. PtNPs/GCE, GNPs/GCE, and MWCNTs/GCE exhibited higher electrochemical responses for FA in comparison with bare GCE as a result of the high conductivity of GNPs, PtNPs, and MWCNTs. PtNPs-GNPs-MWCNTs/GCE exhibited higher peak current and electrochemical activity, indicating that the PtNPs-GNPs-MWCNTs composite greatly facilitated the electron transfer between the solution and the electrode owing to the synergistic effects of PtNPs, GNPs, and MWCNTs. Importantly, the peak current of PtNPs-GNPs-MWCNTs- β -CD/GCE exhibited the highest peak current and electrochemical activity, indicating that the PtNPs-GNPs-MWCNTs- β -CD composite greatly facilitated the electron transfer between the solution and the electrode owing to the synergistic effects of PtNPs, GNPs, MWCNTs, and β -CD.

The electrochemical properties of bare GCE and the modified electrodes were characterized by electrochemical impedance spectroscopy (EIS). As we can see in Fig. 6B, the charge-transfer resistance (R_{ct}) at bare GCE (160.0Ω) was higher than

those at GNPs/GCE (154.9Ω), PtNPs/GCE (130.0Ω), β -CD/GCE (118.7Ω), MWCNTs/GCE (111.3Ω), PtNPs-GNPs-MWCNTs/GCE (110.8Ω), and PtNPs-GNPs-MWCNTs- β -CD/GCE (105.7Ω). Obviously, the R_{ct} of PtNPs-GNPs-MWCNTs- β -CD/GCE was the lowest, which could be attributed to the excellent electrocatalytic activity, high conductivity, and large specific surface area of the electrode modifier, i.e., the assembled PtNPs-GNPs-MWCNTs- β -CD composite. The results were consistent with CVs.

In order to understand the roles of surface area in the electrochemical behavior, CV of bare GCE (Fig. 6C) and PtNPs-GNPs-MWCNTs- β -CD/GCE (Fig. 6E) was studied for $1.0 \text{ mmol L}^{-1} \text{ K}_3[\text{Fe}(\text{CN})_6]$ which was in $0.1 \text{ mol L}^{-1} \text{ KCl}$ at various scan rates ($0.01\text{--}0.30 \text{ V s}^{-1}$). As shown in Fig. 6D, F, the redox peak currents (I_{pa}) of bare GCE and PtNPs-GNPs-MWCNTs- β -CD/GCE were linearly related to the square root of the scan rate, indicating that the mass transfer onto the electrode surface could be a diffusion-controlled process [42, 43]. The electroactive area of bare GCE and PtNPs-GNPs-MWCNTs- β -CD/GCE can be estimated using the Randles-Sevcik equation: $I_{pa} (\mu\text{A}) = (2.69 \times 10^5) n^{3/2} D^{1/2} C A \nu^{1/2} (\text{mV s}^{-1})^{1/2}$ (where n is the number of transferred electrons in the redox reaction of $\text{K}_3[\text{Fe}(\text{CN})_6]$ solution of 1 mmol L^{-1} ; D is the diffusion coefficient of $6.70 \times 10^{-6} \text{ cm}^2 \text{ s}^{-1}$; C is the concentration of $\text{K}_3[\text{Fe}(\text{CN})_6]$ of

Fig. 3 AFM images of the electrodes. **a** Bare GCE. **b** PtNPs-GNPs-MWCNTs- β -CD/GCE

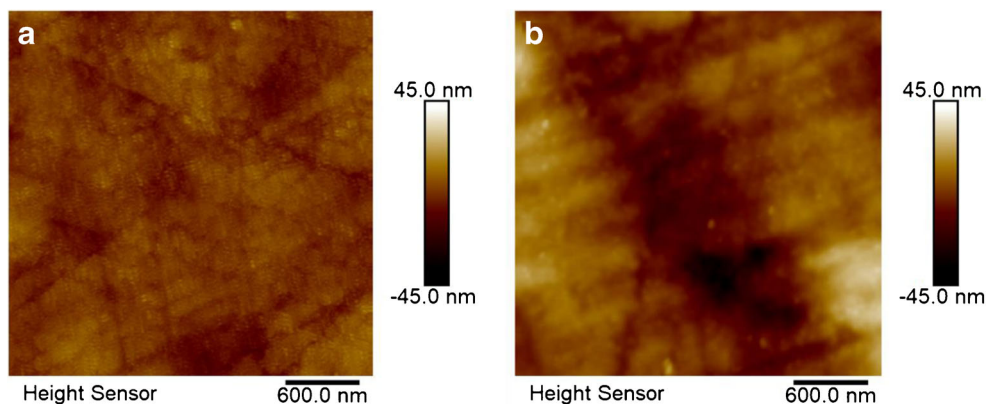
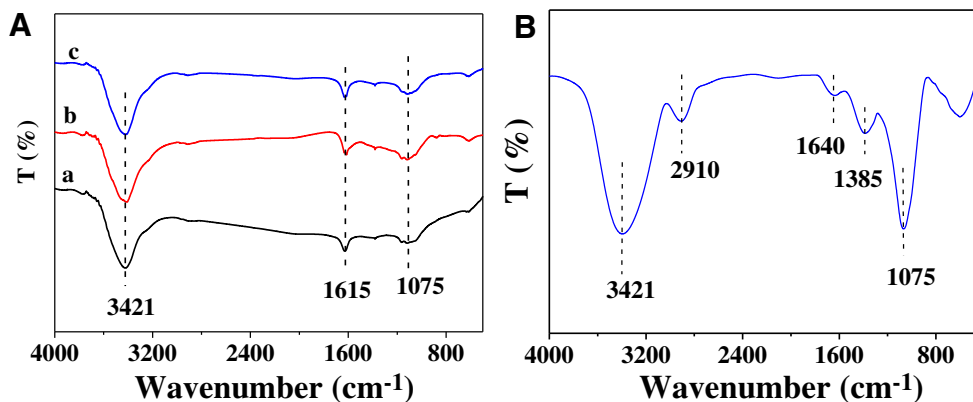


Fig. 4 FT-IR spectra of **A** the carbon-based materials a GNPs, b MWCNTs, c PtNPs-GNPs-MWCNTs- β -CD and **B** β -CD



1 mmol L^{-1} ; A is the electroactive area (cm^2), and ν is the scan rate (mV s^{-1}) [44]. From Fig. 6D, F, the linear equations of I_p and $\nu^{1/2}$ could be expressed as $I_{pa} = 0.95 \nu^{1/2} + 0.92$ and $I_{pa} = 2.32 \nu^{1/2} - 2.28$ at bare GCE and PtNPs-GNPs-MWCNTs- β -CD/GCE, respectively. According to the Randles-Sevcik equation, the electroactive area of bare GCE (0.0436 cm^2) was lower than that of PtNPs-GNPs-MWCNTs- β -CD/GCE (0.105 cm^2), indicating that electron transfer rate could be accelerated at PtNPs-GNPs-MWCNTs- β -CD/GCE.

The effects of scan rate on the peak potential were also investigated. As can be seen from Fig. 6C, E, the separations of the cathodic and anodic peaks at bare GCE and PtNPs-GNPs-MWCNTs- β -CD/GCE increased with an increase in scan rate (10 to 300 mV s^{-1}), suggesting that the redox process was quasi-reversible [45]. The redox peak potentials of bare GCE and PtNPs-GNPs-MWCNTs- β -CD/GCE were plotted against the logarithmic function of scan rates ($\log \nu$), and two linear variations can be observed (Fig. 6G, H). According to Laviron's theory [46], the cathodic and anodic slopes can be presented as $-2.303RT/\alpha nF$ and $2.303RT/(1 - \alpha)nF$, respectively [47], where F is the Faraday constant

($96,485 \text{ C mol}^{-1}$), n is the number of participating electrons ($n = 1$), α is the electron transfer coefficient, T is the temperature (298 K), and R is the ideal gas constant ($8.314 \text{ J K}^{-1} \text{ mol}^{-1}$). On the basis of the slopes of the two straight lines and the equation of $k_a/k_b = (\alpha - 1)/\alpha$ (where k_a and k_b are the slopes of the straight lines for E_{pa} vs. $\log \nu$ and E_{pc} vs. $\log \nu$, respectively), the values of α at bare GCE and PtNPs-GNPs-MWCNTs- β -CD/GCE were calculated to be 0.50 and 0.46, respectively. Furthermore, when the condition of $n\Delta E_p < 200 \text{ mV}$ is fulfilled, the electron transfer rate constant (k_s) under a surface-controlled process can be obtained using Laviron's equation: $\log k_s = \alpha \log(1 - \alpha) + (1 - \alpha) \log \alpha - \log(RT/nF\nu) - nF\alpha(1 - \alpha)\Delta E_p/2.3RT$ (where the scan rate (ν) is 200 mV s^{-1} , ΔE_p is the peak-to-peak potential separation, other parameters are the same as mentioned above) [46]. The k_s of PtNPs-GNPs-MWCNTs- β -CD/GCE (0.903 s^{-1}) was estimated to be higher than that of bare GCE (0.796 s^{-1}), indicating that the PtNPs-GNPs-MWCNTs- β -CD composite contributed to promote the electron transfer between solution and electrode [48].

In addition, the heterogeneous electron transmission rate (k^0) of a quasi-reversible system was estimated by the Nicholson method [49, 50] by using the following equation: $k^0 = \psi [(\pi D n \nu F)/(RT)]^{1/2}$ (where ψ is the dimensionless rate parameter of CV related to ΔE_p : $\psi = (-0.628 + 0.0021\Delta E_p)/(1 - 0.017\Delta E_p)$, other parameters are the same as mentioned above). The values of k^0 at different scan rates calculated by substituting each parameter are listed in Table 1. The average k^0 of PtNPs-GNPs-MWCNTs- β -CD/GCE ($3.10 \times 10^{-3} \text{ cm s}^{-1}$) was higher than that of bare GCE ($2.13 \times 10^{-3} \text{ cm s}^{-1}$), indicating that PtNPs-GNPs-MWCNTs- β -CD possessed higher electrochemical reactivity [50].

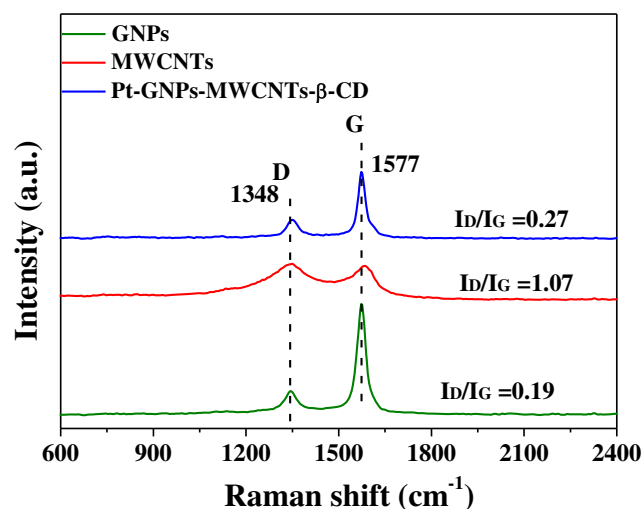
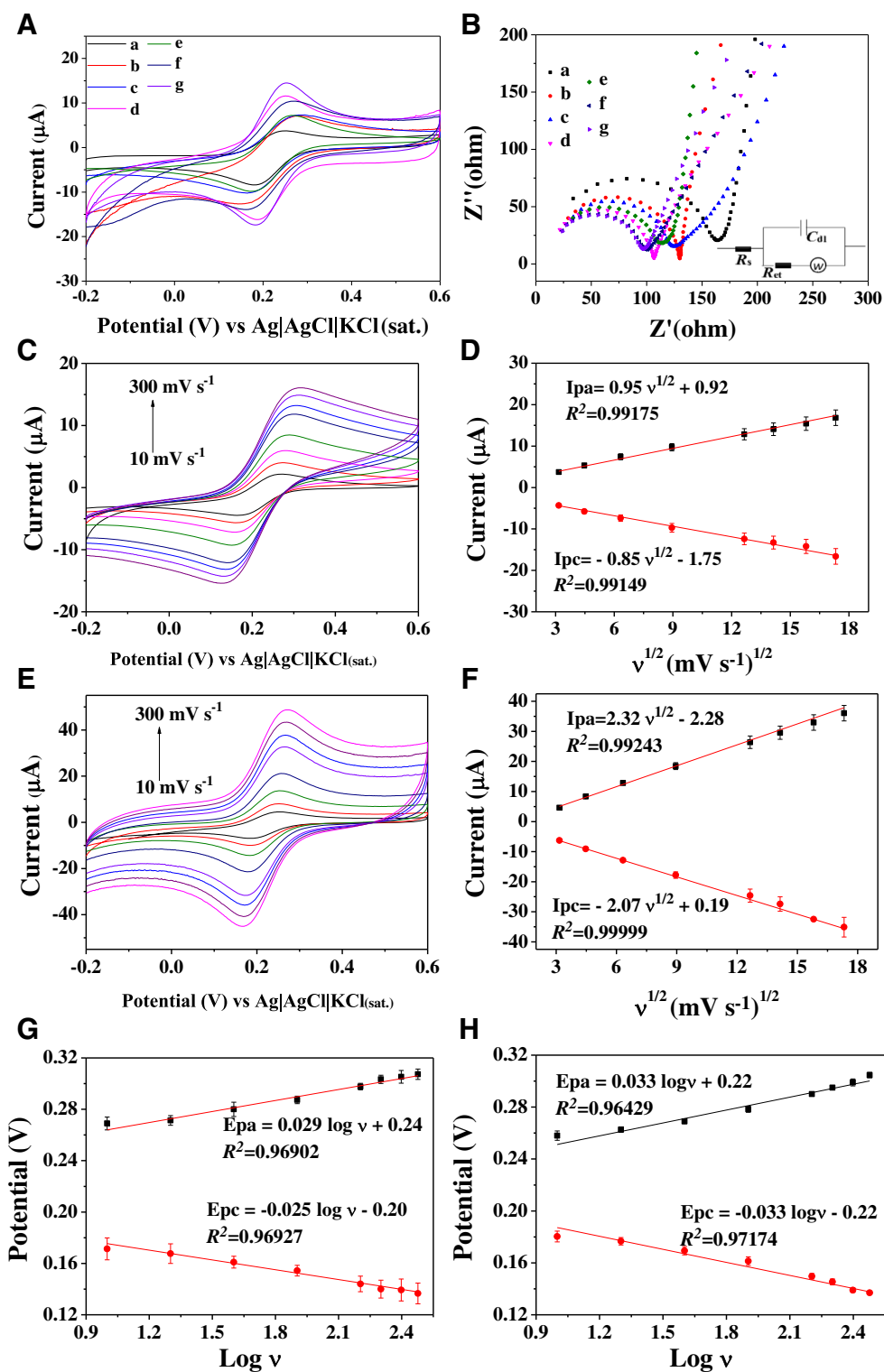


Fig. 5 Raman spectra of GNPs, MWCNTs, and PtNPs-GNPs-MWCNTs- β -CD

Electrochemical behavior of FA

The electrochemical detection of FA at PtNPs-GNPs-MWCNTs- β -CD/GCE by different electrochemical methods including DPV, SWV, and CV was investigated for

Fig. 6 **A** Cyclic voltammograms of different electrodes in $1.0 \text{ mmol L}^{-1} \text{ K}_3[\text{Fe}(\text{CN})_6]$ solution ($0.1 \text{ mol L}^{-1} \text{ KCl}$). **B** Nyquist plots of different electrodes in $1.0 \text{ mmol L}^{-1} \text{ K}_3[\text{Fe}(\text{CN})_6]$ solution ($0.1 \text{ mol L}^{-1} \text{ KCl}$) at open-circuit potential conditions (AC frequency range $0.1\text{--}10^6 \text{ Hz}$, AC amplitude 5.0 mV) (a bare/GCE, b PtNPs/GCE, c GNPs/GCE, d MWCNTs/GCE, e β-CD/GCE, f PtNPs-GNPs-MWCNTs/GCE, g PtNPs-GNPs-MWCNTs-β-CD/GCE). **C** CV of bare GCE in $1.0 \text{ mmol L}^{-1} \text{ K}_3[\text{Fe}(\text{CN})_6]$ solution ($0.1 \text{ mol L}^{-1} \text{ KCl}$) at various scan rates ($0.01, 0.02, 0.04, 0.08, 0.16, 0.20, 0.25,$ and 0.30 V s^{-1}). **D** Plots of redox peak currents versus scan rates at bare GCE (I_{pa} oxidation peak current, I_{pc} reduction peak current). **E** CV of the PtNPs-GNPs-MWCNTs-β-CD/GCE in $1.0 \text{ mmol L}^{-1} \text{ K}_3[\text{Fe}(\text{CN})_6]$ solution (containing $0.1 \text{ mol L}^{-1} \text{ KCl}$) at various scan rates ($0.01, 0.02, 0.04, 0.08, 0.16, 0.20, 0.25,$ and 0.3 V s^{-1}). **F** Plots of the PtNPs-GNPs-MWCNTs-β-CD/GCE redox peak currents as a function of scan rates. Dependence of the redox peak potentials of bare GCE (**G**) and PtNPs-GNPs-MWCNTs-β-CD/GCE (**H**) on $\log \nu$ (E_{pa} oxidation peak potential, E_{pc} reduction peak potential)



comparison (Fig. 7A). The peak current shape of FA by CV was much better than those in DPV and SWV. Moreover, the utilization of DPV and SWV methods would cause the desquamation of coated PtNPs-GNPs-MWCNTs-β-CD film, resulting in severe instability of the electroanalytical data.

Therefore, the CV method was employed in the following electrochemical experiments.

The electrochemical behavior of FA at bare GCE and the modified electrodes was investigated by CV for 0.10 mmol L^{-1} FA which was in 0.1 mol L^{-1} of PBS

Table 1 Bare GCE and PtNPs-GNPs-MWCNTs- β -CD/GCE of ΔE_p and ψ in the Nernst system at 25 °C and the calculated k^0

Bare GCE				PtNPs-GNPs-MWCNTs- β -CD/GCE			
ν (V s ⁻¹)	ΔE_p (mV)	ψ	$10^3 k^0$ (cm s ⁻¹)	ν (V s ⁻¹)	ΔE_p (mV)	ψ	$10^3 k^0$ (cm s ⁻¹)
0.01	97.67	0.64	1.83	0.01	77.67	1.45	4.15
0.02	103.67	0.54	2.18	0.02	86.00	0.97	3.92
0.04	119.00	0.37	2.12	0.04	99.67	0.60	3.45
0.08	133.00	0.28	2.24	0.08	117.00	0.39	3.13
0.16	153.67	0.19	2.17	0.16	140.33	0.24	2.75
0.2	163.33	0.16	2.05	0.2	149.67	0.20	2.60
0.25	166.00	0.15	2.19	0.25	160.00	0.17	2.43
0.3	170.67	0.14	2.22	0.3	167.67	0.15	2.34
Average	—	—	2.13	Average	—	—	3.10

(pH 7.0) in the potential range of 0.2–1.0 V. As shown in Fig. 7B, oxidation of FA at the electrodes was detected and related to the formation of a double bond between C9 and N10 (Scheme 2) [51, 52]. The peak currents of 0.1 mmol L⁻¹ FA (0.1 mol L⁻¹ PBS, pH 7.0) at different electrodes of bare GCE, PtNPs /GCE, GNPs/GCE MWCNTs/GCE, β -CD/GCE, PtNPs-GNPs/GCE, PtNPs-MWCNTs/GCE, PtNPs- β -CD/GCE, GNPs-MWCNTs/GCE, GNPs- β -CD/GCE, MWCNTs- β -CD/GCE, PtNPs-GNPs-MWCNTs/GCE, and PtNPs-GNPs-MWCNTs- β -CD/GCE were 0.78, 1.58, 1.91, 1.57, 0.99, 2.20, 1.86, 1.14, 2.78, 2.16, 4.49, and 4.65 μ A, respectively. The peak currents at the modified electrodes were greatly enhanced owing to the larger specific surface area and the higher conductivity of the working electrodes compared to bare GCE [53]. The aforementioned modified electrode also showed higher oxidation current responses for FA in comparison with bare GCE owing to the high conductivity of GNPs, PtNPs, and MWCNTs. In addition, the peak current at β -CD/GCE was lower, indicating that the insulating β -CD film would prevent the electron transfer rates.

Importantly, when β -CD is present on the surface of GCE, FA would accumulate (preconcentrated) in the β -CD molecular cavities, so the surface concentration of FA is higher than that in the bulk solution. Therefore, the CV peak currents in the presence of β -CD on the surface of GCE are higher than those in the absence of β -CD. Moreover, the highest peak current could be obtained at PtNPs-GNPs-MWCNTs- β -CD/GCE, indicating that it possessed excellent electrocatalytic activity towards FA. The high conductivity and the large electroactive surface area of PtNPs-GNPs-MWCNTs- β -CD/GCE, as well as the synergistic effects of PtNPs, GNPs, MWCNTs, and β -CD were beneficial to the electrochemical detection of FA [54].

Optimization of analytical conditions

Effects of amount of coated PtNPs-GNPs-MWCNTs- β -CD

The electrochemical responses of FA at modified GCE with various amounts of PtNPs-GNPs-MWCNTs- β -CD were

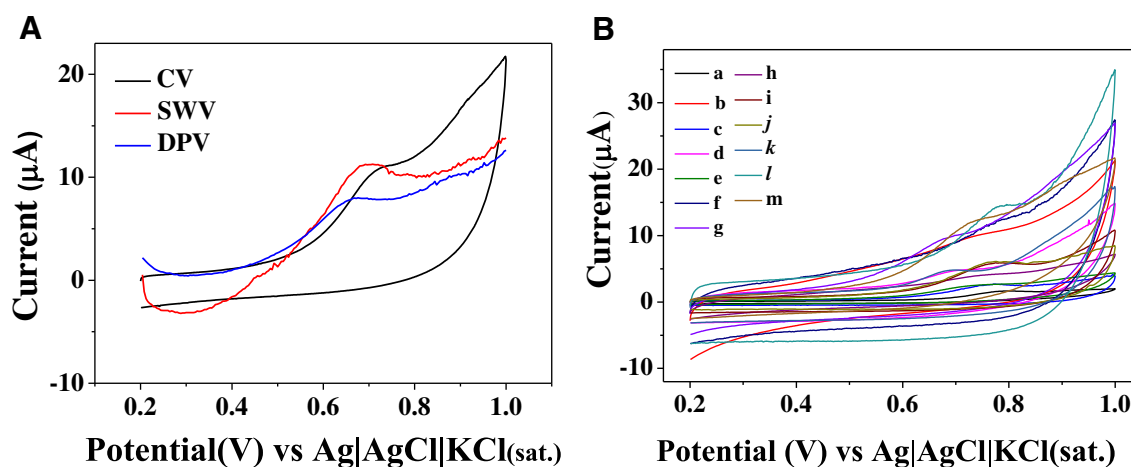
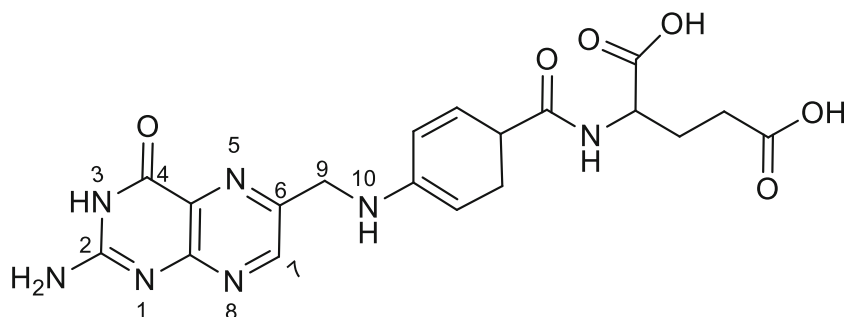


Fig. 7 **A** Electrochemical behavior of 0.1 mmol L⁻¹ FA (0.1 M PBS, pH 7.0) using different electrochemical techniques. **B** CVs of different electrodes in 0.10 mmol L⁻¹ of FA solution (0.1 mol L⁻¹ of PBS as supporting electrolyte): a bare/GCE, b PtNPs/GCE, c GNPs/GCE d

MWCNTs/GCE, e β -CD/GCE f PtNPs-GNPs/GCE, g PtNPs-MWCNTs/GCE, h PtNPs- β -CD/GCE, i GNPs-MWCNTs/GCE, j GNPs- β -CD/GCE, k MWCNTs- β -CD/GCE, l PtNPs-GNPs-MWCNTs/GCE, and m PtNPs-GNPs-MWCNTs- β -CD/GCE

Scheme 2 Structure of FA



investigated by CV. As we can see in Fig. 8, the peak current of FA gradually increased to a maximum value and then decreased when the amount of coated PtNPs-GNPs-MWCNTs- β -CD gradually from 5.0 μL to 10.0 μL . The electrode cannot be completely covered if the amount of coated PtNPs-GNPs-MWCNTs- β -CD is too small, and the peak current response would decrease. An excess amount of coated PtNPs-GNPs-MWCNTs- β -CD would increase the thickness of the film, and the peak current response at PtNPs-GNPs-MWCNTs- β -CD/GCE decreased because of the hindered electron transfer between the electrode and FA. The peak current of FA at the modified GCE reached to a maximum when the amount of coated PtNPs-GNPs-MWCNTs- β -CD composite was 7.0 μL . Thus, the optimal amount of coated PtNPs-GNPs-MWCNTs- β -CD suspension was set as 7.0 μL .

Effects of pH

The pH of buffer solution (0.1 mol L⁻¹ of PBS) has an important impact on the electrochemical behavior of FA at the modified GCE. The electrochemical detection of FA at PtNPs-GNPs-MWCNTs- β -CD/GCE in PBS solutions with different

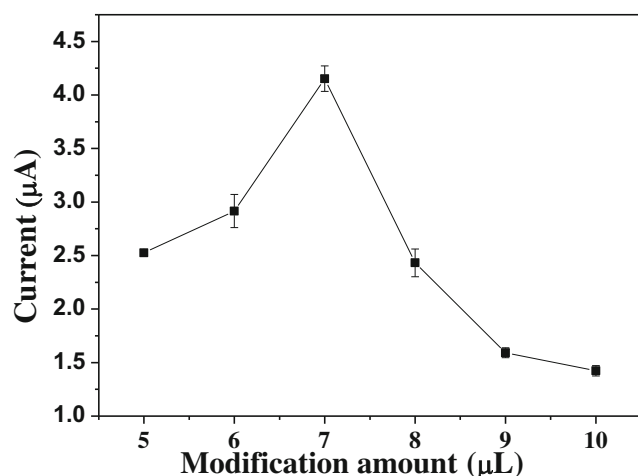


Fig. 8 Effects of amount of coated PtNPs-GNPs-MWCNTs- β -CD on the electrochemical responses of modified GCE toward FA

pH values of 4.0, 5.0, 6.0, 7.0, 8.0, and 9.0 was investigated (Fig. 9). The oxidation peak currents of FA gradually increased with an increase in pH value of PBS and reached a maximum at pH 7.0 and then declined thereafter. FA was unionized in an acid medium and not susceptible to electrochemical oxidation because of its low pK_{a1} (2.3) [55]. The largest oxidation peak current could be obtained at PtNPs-GNPs-MWCNTs- β -CD/GCE for FA at pH 7.0, indicating that FA underwent an efficient electrochemical oxidation. Anionic forms of FA would appear when the pH is higher than 7.0 (pK_{a2} = 8.3), again resulting in a decrease in oxidation peak current [56]. Therefore, PBS of pH 7.0 was used in the following experiments.

Effects of scan rate

To evaluate the effect of electrochemical surface properties of PtNPs-GNPs-MWCNTs- β -CD/GCE on determination of FA, CV investigation was performed at various scan rates (0.01–0.3 V s⁻¹) in 0.1 mmol L⁻¹ FA in 0.1 mol L⁻¹ PBS (pH 7.0) at a potential range of 0.2–1.0 V. As shown in Fig. 10, the oxidation peak current of FA increased with an increasing scan rate, and the linear regression equation could be expressed as $I_{pa} = 19.18 \nu^{1/2} - 0.33$ ($R^2 = 0.9906$). The oxidation peak current was proportional to the square root of scan rate ($\nu^{1/2}$), and the current at the modified electrodes conformed to the Randles-Sevcik equation [57]. The results showed that the reversible redox of FA at PtNPs-GNPs-MWCNTs- β -CD/GCE might be controlled by the rate of bulk diffusion [58].

Determination of FA

Under the optimized experimental conditions, a series of FA solutions with different concentrations (0.02–0.50 mmol L⁻¹) were tested by CV at PtNPs-GNPs-MWCNTs- β -CD/GCE in 0.1 mol L⁻¹ of PBS (pH 7.0) (Fig. 11). The peak currents linearly increased with an increase in FA concentrations in the range 0.02–0.50 mmol L⁻¹ (Fig. 11, inset). A linear equation of $I_{pa} (\mu\text{A}) = 24.83 C_{FA} (\text{mmol L}^{-1}) + 0.097$ ($R^2 = 0.9942$) could be obtained, and the limit of detection (LOD) was estimated to be 0.48 $\mu\text{mol L}^{-1}$ (signal-to-noise ratio = 3).

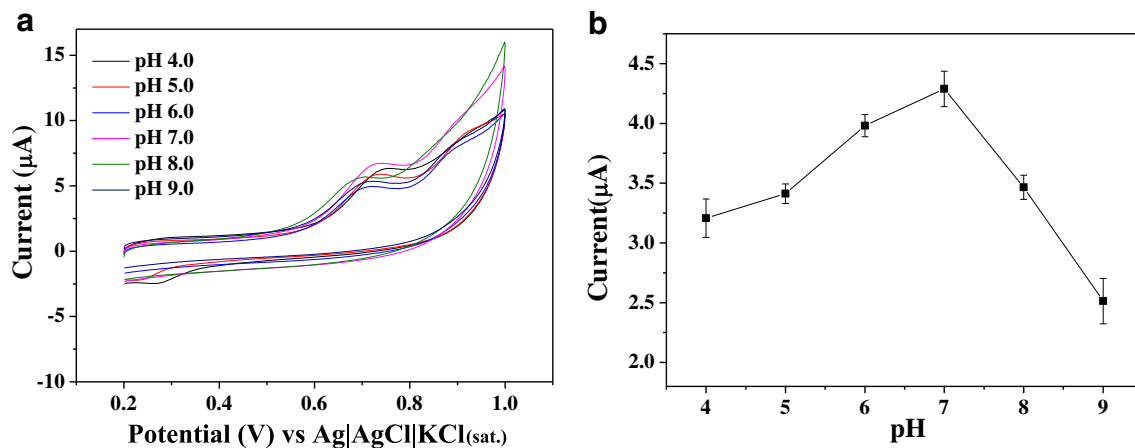


Fig. 9 **a** CV behavior of 0.1 mmol L⁻¹ FA (containing 0.1 mol L⁻¹ of PBS) with different pH values. **b** Effects of pH value (4.0, 5.0, 6.0, 7.0, 8.0, and 9.0) on peak current response of 0.1 mmol L⁻¹ FA (containing 0.1 mol L⁻¹ of PBS)

The LOD and the linear dynamic concentration range of PtNPs-GNPs-MWCNTs- β -CD/GCE for the detection of FA were compared with some previously reported electrodes. As shown in Table 2, PtNPs-GNPs-MWCNTs- β -CD/GCE possessed lower LOD and wider linearity range. Therefore, the developed electrode is of considerable practical value for measuring FA owing to its advantages including greater simplicity, higher sensitivity, and wider linear range.

Anti-interference ability and stability

The anti-interference ability of PtNPs-GNPs-MWCNTs- β -CD/GCE for detection of FA was evaluated. The influence of some potential coexisting interfering species including NaCl (5.0 mmol L⁻¹), KCl (5.0 mmol L⁻¹), MgCl₂ (5.0 mmol L⁻¹), CaCl₂ (5.0 mmol L⁻¹), Zn(NO₃)₂ (5.0 mmol L⁻¹), glucose (1.0 mmol L⁻¹), and glutamate (1.0 mmol L⁻¹) with FA (0.1 mmol L⁻¹) in 0.1 mol L⁻¹ PBS

at PtNPs-GNPs-MWCNTs- β -CD/GCE was investigated. Generally, the current ratio (%) is used to evaluate the anti-interference ability of the electrode, and the current ratio (%) is defined as the difference between the currents of the target object measured before and after the addition of the interfering substance. Figure 12 shows that these potential interfering agents at 10-fold or 50-fold higher concentrations than that of FA had little influence on the response signals of FA and the current ratios (%) were less than 6.16%. The results indicated that the proposed PtNPs-GNPs-MWCNTs- β -CD/GCE possessed excellent anti-interference ability.

The stability of PtNPs-GNPs-MWCNTs- β -CD/GCE was studied by CV in 0.1 mmol L⁻¹ FA. The intra-day and inter-day precisions of PtNPs-GNPs-MWCNTs- β -CD/GCE for FA were investigated for 5 times in one day and in five consecutive days at the same electrode, respectively. Then the relative standard deviations (RSD) of intra-day precision and inter-day precision ($n = 5$) of PtNPs-

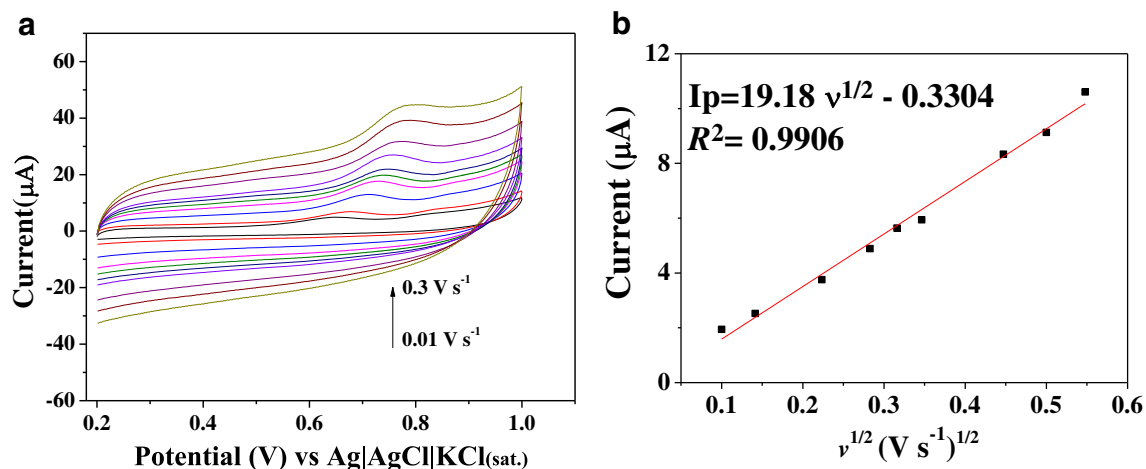


Fig. 10 **a** Cyclic voltammograms of PtNPs-GNPs-MWCNTs- β -CD/GCE for FA (0.1 mmol L⁻¹) solution at different scan rates (0.01, 0.02, 0.05, 0.08, 0.10, 0.12, 0.20, 0.25, and 0.30 V s⁻¹). **b** Plots of oxidation peak current versus square root of scan rate ($v^{1/2}$) at PtNPs-GNPs-MWCNTs- β -CD/GCE

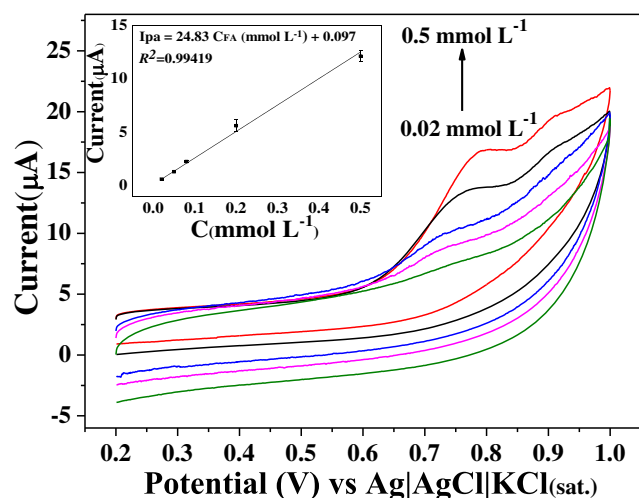


Fig. 11 CV behavior of PtNPs-GNPs-MWCNTs-β-CD/GCE in FA (0.1 mol L^{-1} PBS pH 7.0) in the concentration range $0.02\text{--}0.50 \text{ mmol L}^{-1}$ (inset plot of peak current versus FA concentration)

GNPs-MWCNTs-β-CD/GCE toward FA were 5.19% and 6.07%, respectively. Therefore, the developed PtNPs-GNPs-MWCNTs-β-CD/GCE exhibited good stability and reproducibility for the determination of FA.

Determination of FA in real samples

In order to evaluate the sensitivity and practical applicability of the proposed PtNPs-GNPs-MWCNTs-β-CD/GCE, the determination of FA in actual samples, FA tablets, was performed. FA tablets (0.40 mg per pill) were purchased from a local pharmacy (Changsha, China). FA tablets were crushed and dissolved in 10 mL of 0.1 mol L^{-1} PBS (pH 7.0), and the standard addition method was used for the accurate determination. The spiked recoveries were in the range 97.55–102.96% and RSDs were in the range 2.07–4.64% (Table 3). Therefore, the proposed PtNPs-GNPs-MWCNTs-β-CD/GCE can be used for the determination of FA in real samples with

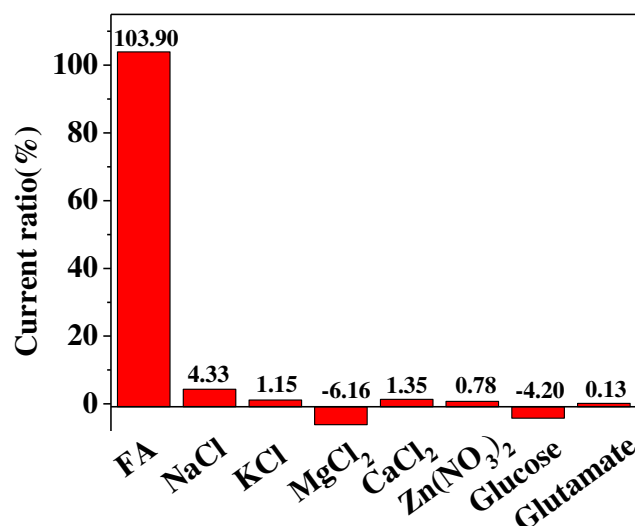


Fig. 12 Amperometric current response of PtNPs-GNPs-MWCNTs-β-CD/GCE for 0.1 mM FA containing some potential interfering substances including NaCl (5.0 mmol L^{-1}), KCl (5.0 mmol L^{-1}), MgCl_2 (5.0 mmol L^{-1}), CaCl_2 (5.0 mmol L^{-1}), $\text{Zn}(\text{NO}_3)_2$ (5.0 mmol L^{-1}), glucose (1.0 mmol L^{-1}), and glutamate (1.0 mmol L^{-1}) in PBS (0.1 mol L^{-1} , pH 7.0)

relatively high accuracy and precision and relatively high linear correlation.

Conclusion

In this work, a novel nanocomposite-based sensor, PtNPs-GNPs-MWCNTs-β-CD/GCE, was successfully fabricated and used for the electrochemical detection of FA by CV. Under the optimum experimental conditions, PtNPs-GNPs-MWCNTs-β-CD/GCE showed higher electrochemical responses for FA in 0.1 mol L^{-1} PBS solution, and relatively high linear correlation between oxidation peak current and FA concentration in the range of $0.02\text{--}0.50 \text{ mmol L}^{-1}$ could be

Table 2 Comparison of previously reported electrochemical sensors and PtNPs-GNPs-MWCNTs-β-CD/GCE for detection of FA

Electrode	Method	LOD ($\mu\text{mol L}^{-1}$)	Linear range ($\mu\text{mol L}^{-1}$)	Ref.
AuNCs/AGR/MWCNT/GCE	SWV	0.09	10–170	[53]
MDWCNTPE	DPV	11.0	15–800	[59]
$\text{Co}_3\text{O}_4/\text{rGO}/\text{CTAB}$	DPV	19.0	300–3200	[10]
PAIUCPE	LSV	0.15	0.2–3.0	[60]
ZONMCPE	DPV	9.86	20–2500	[61]
MB/ERGO/GCE	DPV	0.50	4.0–167	[62]
PtNPs-GNPs-MWCNTs-β-CD/GCE	CV	0.48	20–500	This work

AuNCs/AGR/MWCNT gold nanoclusters/activated graphene/MWCNT nanocomposite, MDWCNTPE 2,2'-[1,2-ethanediybis(nitriloethylidene)]-bis-hydroquinone double-wall carbon nanotube paste electrode, $\text{Co}_3\text{O}_4/\text{rGO}/\text{CTAB}$ cobalt oxide-reduced graphene oxide-cetyltrimethyl ammonium bromide modified carbon paste electrode, PAIUCPE pre-anodized inlaying ultrathin carbon paste electrode, ZONMCPE ZrO_2 nanoparticles-modified carbon paste electrode, MB/ERGO methylene blue/electrodeposited reduced graphene oxide

Table 3 Determination of FA in FA tablet ($n = 3$)

Real samples	Added (mmol L ⁻¹)	Found (mmol L ⁻¹)	Recovery (%)	RSD (%)
FA tablets	–	0.110	–	3.96
	0.05	0.161	102.96	2.07
	0.10	0.207	97.55	4.64
	0.15	0.262	101.52	2.31

obtained. The LOD was evaluated to be 0.48 $\mu\text{mol L}^{-1}$. The recoveries of determination of FA in FA tablets were calculated to be 97.55–102.96%. Therefore, PtNPs-GNPs-MWCNTs- β -CD/GCE could be used to accurately determine FA, and it provides a platform for the detection of FA in real samples.

Acknowledgments The authors are grateful for financial support from National Natural Science Foundation of China (Grant No. 51674292) and Provincial Natural Science Foundation of Hunan (Grant No. 2016JJ1023).

Compliance with ethical standards

Conflict of interest The authors declare that they have no conflicts of interest.

References

- Herbert V. Folic acid. *Annu Rev Med.* 1965;16(1):359–70.
- Catala GN, Bestwick CS, Russell WR, Tortora K, Giovannelli L, Moyer MP, et al. Folate, genomic stability and colon cancer: the use of single cell gel electrophoresis in assessing the impact of folate in vitro, in vivo and in human biomonitoring. *Mutat Res.* 2019;843:73–80.
- Navarrete-Muñoz EM, Valera-Gran D, Garcia-de-la-Hera M, Gonzalez-Palacios S, Riaño I, Murcia M, et al. High doses of folic acid in the periconceptional period and risk of low weight for gestational age at birth in a population based cohort study. *Eur J Nutr.* 2019;58(1):241–51.
- Wang F, Cao M, Wang N, Muhammad N, Wu S, Zhu Y. Simple coupled ultrahigh performance liquid chromatography and ion chromatography technique for simultaneous determination of folic acid and inorganic anions in folic acid tablets. *Food Chem.* 2018;239:62–7.
- Wang M, Jiao Y, Cheng C, Hua J, Yang Y. Nitrogen-doped carbon quantum dots as a fluorescence probe combined with magnetic solid-phase extraction purification for analysis of folic acid in human serum. *Anal Bioanal Chem.* 2017;409(30):7063–75.
- Bertuzzi T, Rastelli S, Mulazzi A, Rossi F. LC-MS/MS determination of mono-glutamate folates and folic acid in beer. *Food Anal Method.* 2019;12(3):722–8.
- Cao Y, Griffith B, Bhomkar P, Wishart DS, McDermott MT. Functionalized gold nanoparticle-enhanced competitive assay for sensitive small-molecule metabolite detection using surface plasmon resonance. *Analyst.* 2018;143(1):289–96.
- Hoyos-Arbeláez J, Vázquez M, Contreras-Calderón J. Electrochemical methods as a tool for determining the antioxidant capacity of food and beverages: a review. *Food Chem.* 2017;221:1371–81.
- Kıranşan KD, Topçu E. Free-standing and flexible MoS₂/rGO paper electrode for amperometric detection of folic acid. *Electroanal.* 2018;30(5):810–8.
- Venu M, Agarwa VKGS, Venkateswarlu S, Madhavi G. Simultaneous determination of dopamine, uric acid and folic acid with electrochemical techniques based on Co₃O₄/rGO/CTAB modified carbon paste electrode. *Int J Electrochem Sci.* 2018;13:11702–19.
- Tahernejad-Javazmi F, Shabani-Nooshabadi M, Karimi-Maleh H. 3D reduced graphene oxide/FeNi₃-ionic liquid nanocomposite modified sensor; an electrical synergic effect for development of tert-butylhydroquinone and folic acid sensor. *Compos Part B-Eng.* 2019;172:666–70.
- Wong A, Santos AM, Silva TA, Fatibello-Filho O. Simultaneous determination of isoproterenol, acetaminophen, folic acid, propranolol and caffeine using a sensor platform based on carbon black, graphene oxide, copper nanoparticles and PEDOT: PSS. *Talanta.* 2018;183:329–38.
- Gao X, Yue H, Huang S, Lin X, Gao XP, Wang B, et al. Synthesis of graphene/ZnO nanowire arrays/graphene foam and its application for determination of folic acid. *J Electroanal Chem.* 2018;808:189–94.
- Akbar S, Anwar A, Kanwal Q. Electrochemical determination of folic acid: a short review. *Anal Biochem.* 2016;510:98–105.
- Freeman R, Finder T, Bahshi L, Willner I. β -Cyclodextrin-modified CdSe/ZnS quantum dots for sensing and chiroselective analysis. *Nano Lett.* 2009;9(5):2073–6.
- Ares AM, Muino R, Costoya A, Lorenzo RA, Concheiro A, Carro AM, et al. Cyclodextrin-functionalized cellulose filter paper for selective capture of diclofenac. *Carbohydr Polym.* 2019;220:43–52.
- Wang KR, Guo DS, Jiang BP, Sun ZH, Liu Y. Molecular aggregation behavior of perylene-bridged bis(β -cyclodextrin) and its electronic interactions upon selective binding with aromatic guests. *J Phys Chem B.* 2010;114(1):101–6.
- Michalska K, Gruba E, Bocian W, Cielecka-Piontek J. Enantioselective recognition of radezolid by cyclodextrin modified capillary electrokinetic chromatography and electronic circular dichroism. *J Pharm Biomed Anal.* 2017;139:98–108.
- Zou J, Yu JG. Chiral recognition of tyrosine enantiomers on a novel bis-aminosaccharides composite modified glassy carbon electrode. *Anal Chim Acta.* 2019;1088:35–44.
- Ceborska M, Zimnicka M, Wszelaka-Rylik M, Troć A. Characterization of folic acid/native cyclodextrins host-guest complexes in solution. *J Mol Struct.* 2016;1109:114–8.
- Nekvinda J, Grüner B, Gabel D, Nau WM, Assaf KI. Host-guest chemistry of carboranes: synthesis of carboxylate derivatives and their binding to cyclodextrins. *Chem-Eur J.* 2018;24(49):12970–5.
- Tan L, Zhou KG, Zhang YH, Wang HX, Wang XD, Guo YF, et al. Nanomolar detection of dopamine in the presence of ascorbic acid at β -cyclodextrin/graphene nanocomposite platform. *Electrochem Commun.* 2010;12(4):557–60.
- Britto PJ, Santhanam KSV, Rubio A, Alonso JA, Ajayan PM. Improved charge transfer at carbon nanotube electrodes. *Adv Mater.* 1999;11(2):154–7.
- Wu W, Jia M, Zhang Z, Chen X, Zhang Q, Zhang W, et al. Sensitive, selective and simultaneous electrochemical detection of

- multiple heavy metals in environment and food using a lowcost Fe_3O_4 nanoparticles/fluorinated multi-walled carbon nanotubes sensor. *Ecotox Environ Saf.* 2019;175:243–50.
25. Shetti NP, Malode SJ, Nayak DS, Aminabhavi TM, Reddy KR. Nanostructured silver doped TiO_2/CNTs hybrid as an efficient electrochemical sensor for detection of anti-inflammatory drug, cetirizine. *Microchem J.* 2019;150:104124.
 26. Razavipanah I, Rounaghi GH, Deiminat B, Damirchi S, Abnous K, Izadyar M, et al. A new electrochemical aptasensor based on MWCNT- $\text{SiO}_2@Au$ core-shell nanocomposite for ultrasensitive detection of bisphenol A. *Microchem J.* 2019;146:1054–63.
 27. Kang X, Wang J, Wu H, Liu J, Aksay IA, Lin Y. A graphene-based electrochemical sensor for sensitive detection of paracetamol. *Talanta.* 2010;81(3):754–9.
 28. Liao C, Zhao XR, Jiang XY, Teng J, Yu JG. Hydrothermal fabrication of novel three-dimensional graphene oxide-pentaerythritol composites with abundant oxygen-containing groups as efficient adsorbents. *Microchem J.* 2020;152:104288.
 29. Zhu Y, Zeng GM, Zhang Y, Tang L, Chen J, Cheng M, et al. Highly sensitive electrochemical sensor using a MWCNTs/GNPs-modified electrode for lead (II) detection based on $\text{Pb}^{(2+)}$ -induced G-rich DNA conformation. *Analyst.* 2014;139(19):5014–20.
 30. Akilarasan M, Kogularasu S, Chen SM, Chen TW, Lin SH. One-step synthesis of reduced graphene oxide sheathed zinc oxide nanoclusters for the trace level detection of bisphenol A in tissue papers. *Ecotox Environ Saf.* 2018;161:699–705.
 31. Zou J, Yuan MM, Huang ZN, Chen XQ, Jiang XY, Jiao FP, et al. Highly-sensitive and selective determination of bisphenol A in milk samples based on self-assembled graphene nanoplatelets-multiwalled carbon nanotube-chitosan nanostructure. *Mat Sci Eng C-Mater.* 2019;103.
 32. Guan JF, Huang ZN, Zou J, Jiang XY, Peng DM, Yu JG. A sensitive non-enzymatic electrochemical sensor based on acicular manganese dioxide modified graphene nanosheets composite for hydrogen peroxide detection. *Ecotox Environ Saf.* 2020;190:110123.
 33. Li S, Liao L, Wu R, Yang Y, Xu L, Xiao X, et al. Resonance light scattering detection of fructose bisphosphates using uranyl-salophen complex-modified gold nanoparticles as optical probe. *Anal Bioanal Chem.* 2015;407(29):8911–8.
 34. Huang ZN, Jiao Z, Teng J, Liu Q, Yuan MM, Jiao FP, et al. A novel electrochemical sensor based on self-assembled platinum nanochains - multi-walled carbon nanotubes-graphene nanoparticles composite for simultaneous determination of dopamine and ascorbic acid. *Ecotox Environ Saf.* 2019;172:167–75.
 35. Polsky R, Gill R, Kaganovsky L, Willner I. Nucleic acid-functionalized Pt nanoparticles: catalytic labels for the amplified electrochemical detection of biomolecules. *Anal Chem.* 2006;78(7):2268–71.
 36. Guo S, Wen D, Zhai Y, Dong S, Wang E. Platinum nanoparticle ensemble-on-graphene hybrid nanosheet: one-pot, rapid synthesis, and used as new electrode material for electrochemical sensing. *ACS Nano.* 2010;4(7):3959–68.
 37. Zhong X, Feng Y, Lieberwirth I, Knoll W. Facile synthesis of morphology-controlled platinum nanocrystals. *Chem Mater.* 2006;18:2468–71.
 38. Xu F, Sun Y, Zhang Y, Shi Y, Wen Z, Li Z. Graphene-Pt nanocomposite for nonenzymatic detection of hydrogen peroxide with enhanced sensitivity. *Electrochem Commun.* 2011;13(10):1131–4.
 39. Shinde VV, Jeong D, Jung S. Supramolecular aminocatalysis via inclusion complex: amino-doped β -cyclodextrin as an efficient supramolecular catalyst for the synthesis of chromeno pyrimido[1,2-b]indazol in water. *J Ind Eng Chem.* 2018;68:6–13.
 40. Zhou Y, Bao Q, Tang LAL, Zhong Y, Loh KP. Hydrothermal dehydration for the “green” reduction of exfoliated graphene oxide to graphene and demonstration of tunable optical limiting properties. *Chem Mater.* 2009;21(13):2950–6.
 41. Chen Z, Wei P, Zhang S, Lu B, Zhang L, Yang X, et al. Graphene reinforced nickel-based superalloy composites fabricated by additive manufacturing. *Mater Sci Eng A.* 2020;769:138484.
 42. Watanabe T, Einaga Y. Design and fabrication of nickel microdisk-arrayed diamond electrodes for a non-enzymatic glucose sensor based on control of diffusion profiles. *Biosens Bioelectron.* 2009;24(8):2684–9.
 43. Eddowes MJ, Hill HAO. Electrochemistry of horse heart cytochrome c. *J Am Chem Soc.* 1979;101:4461–4.
 44. Mukherjee R, Krishnan R, Lu TM, Koratkar N. Nanostructured electrodes for high-power lithium ion batteries. *Nano Energy.* 2012;1(4):518–33.
 45. Ghreera AS. Quantum dot modified interface for electrochemical immunosensing of procalcitonin for the detection of urinary tract infection. *Anal Chim Acta.* 2019;1056:26–33.
 46. Laviron E. General expression of the linear potential sweep voltammogram in the case of diffusionless electrochemical systems. *J Electroanal Chem.* 1979;101:19–28.
 47. Luong JHT, Glennon JD, Gedanken A, Vashist SK. Achievement and assessment of direct electron transfer of glucose oxidase in electrochemical biosensing using carbon nanotubes, graphene, and their nanocomposites. *Microchim Acta.* 2016;184(2):369–88.
 48. Sun W, Gong S, Shi F, Cao L, Ling L, Zheng W, et al. Direct electrochemistry and electrocatalysis of hemoglobin in graphene oxide and ionic liquid composite film. *Mater Sci Eng C Mater Biol Appl.* 2014;40:235–41.
 49. Thakur B, Bernalte E, Smith J, Linton P, Sawant S, Banks C, et al. The mediatorless electroanalytical sensing of sulfide utilizing unmodified graphitic electrode materials. *C J Carbon Res.* 2016;2(2):14.
 50. Nicholson RS. Theory and application of cyclic voltammetry for measurement of electrode reaction kinetics. *Anal Chem.* 1965;37:1351–5.
 51. Kun Z, Ling Z, Yi H, Ying C, Dongmei T, Shuliang Z, et al. Electrochemical behavior of folic acid in neutral solution on the modified glassy carbon electrode: platinum nanoparticles doped multi-walled carbon nanotubes with Nafion as adhesive. *J Electroanal Chem.* 2012;677-680:105–12.
 52. Xiao F, Ruan C, Liu L, Yan R, Zhao F, Zeng B. Single-walled carbon nanotube-ionic liquid paste electrode for the sensitive voltammetric determination of folic acid. *Sensor Actuator B Chem.* 2008;134(2):895–901.
 53. Abdelwahab AA, Shim YB. Simultaneous determination of ascorbic acid, dopamine, uric acid and folic acid based on activated graphene/MWCNT nanocomposite loaded Au nanoclusters. *Sensor Actuator B Chem.* 2015;221:659–65.
 54. Dai H, Li Y, Zhang S, Gong L, Li X, Lin Y. Delicate photoelectrochemical sensor for folic acid based on carbon nanohorns supported interwoven titanate nanotubes. *Sensor Actuator B Chem.* 2016;222:120–6.
 55. Moorthy PN, Hayon E. One-electron redox reactions of water-soluble vitamins. II. Pterin and folic acid. *J Org Chem.* 1976;41(7):1607–13.
 56. Akhtar MJ, Khan MA, Ahmad I. Photodegradation of folic acid in aqueous solution. *J Pharmaceut Biomed.* 1999;25:269–75.
 57. Saus W, Knittel D, Schollmeyer E. Voltammetric determination of reducing agents and dyestuffs in textile printing pastes. *Fresenius J Anal Chem.* 1990;338(8):912–6.

58. He L, Wang Q, Mandler D, Li M, Boukherroub R, Szunerits S. Detection of folic acid protein in human serum using reduced graphene oxide electrodes modified by folic-acid. *Biosens Bioelectron.* 2016;75:389–95.
59. Beitollahi H, Ardakani MM, Ganjipour B, Naeimi H. Novel 2,2'-[1,2-ethanediylbis(nitriloethylidene)]-bis-hydroquinone double-wall carbon nanotube paste electrode for simultaneous determination of epinephrine, uric acid and folic acid. *Biosens Bioelectron.* 2008;24(3):362–8.
60. Je H, Shangguan E, Li Q. A pre-anodized inlaying ultrathin carbon paste electrode for simultaneous determination of uric acid and folic acid. *Electrochim Acta.* 2013;89:600–6.
61. Mazloun-Ardakani M, Beitollahi H, Amini MK, Mirkhalaf F, Abdollahi-Alibeik M. New strategy for simultaneous and selective voltammetric determination of norepinephrine, acetaminophen and folic acid using ZrO₂ nanoparticles-modified carbon paste electrode. *Sensor Actuator B Chem.* 2010;151(1):243–9.
62. Zhang D, Ouyang X, Ma W, Li L, Zhang Y. Voltammetric determination of folic acid using adsorption of methylene blue onto electrodeposited of reduced graphene oxide film modified glassy carbon electrode. *Electroanal.* 2016;28(2):312–9.

Publisher's note Springer Nature remains neutral with regard to jurisdictional claims in published maps and institutional affiliations.